DOI: http://dx.doi.org/10.1177/1099636213512497

EFFECT OF NANOFILLERS ON LOW ENERGY IMPACT PERFORMANCE OF SANDWICH STRUCTURES WITH NANOREINFORCED POLYURATHANE FOAM CORES

SOPHIA SACHSE[1], MANOHAR PORURI[1], FRANCESCO SILVA[1], SLAWOMIR MICHALOWSKI[2], KRZYSZTOF PIELICHOWSKI[2] and JAMES NJUGUNA[3*]

[1] Centre for Automotive Technology, Cranfield University, Bedfordshire MK43 0AL, UK

[3] Department of Chemistry and Technology of Polymers, Cracow University of Technology, Ul. Warszawska 24, 31-155 Krakow, Poland

[3]Institute for Innovation, Design and Sustainability, School of Engineering Robert Gordon University, Aberdeen, AB25 1HG, UK

[*]Corresponding Author: Email. j.njuguna@rgu.ac.uk; Tel. T: +44 (0) 122 426 2304 (J. Njuguna)

ABSTRACT. Sandwich panels were fabricated with nanoclay filled polyurethane foams and glass fiber reinforced polyamide (PA6) and polypropylenes (PP) face sheets. Nanoclay filled foam cores, with organophilic montmorillonite loadings of 0-10 wt.%, were synthesised through polyaddition of the polyol premix with 4,4'-diphenylmethane diisocyanate, and bound to the injected moulded face sheets. Produced sandwich structures were then subjected to low energy impact (15J) tests under localised point and surface loads, in an instrumented impact test setup. Additionally, quasi static compressive behaviour of the sandwiches panels was studied. The results showed that the addition of nanoclay in the PU foam core, improved both energy absorption and maximal deflection during impact. The improvement in energy absorption was between 66-92% for PP face sheet sandwiches and 23-34% for the PA6 face sheet sandwiches during point load. Furthermore, an increase of the compression modulus of 20-37% was recorded for the sandwiches with PA6 face sheets.

KEYWORDS. nanocomposites, sandwich structures , polyurethane core , low energy impact , damage

1. INTRODUCTION

High specific strength and stiffness, low weight, excellent thermal insulation, acoustic sampling, and fire retardancy are just some of the excellent properties sandwich structures have to offer in structural applications. Hence, sandwich structures are commonly used in many industries such as aerospace, marine, automobile, locomotive, windmills, building, and consumer industries among others. Despite all these advantages, sandwich composites suffer sensitivity to impact loading damage, and thus are limited in their function. Low energy impact can cause structural damage to the core material, whilst the face sheet remains undamaged. If the damage to the core material remains undetected, a potential risk for the application arises. This is imaginable for real life scenarios such as; tool dropping, runway debris, bird strikes, hailstorms and ballistic loading. Therefore, it is crucial to improve the damage resistance characterizes of sandwich structures. The damage initiation thresholds and damage size in sandwich structures primarily depend on the properties of the core materials and face sheets and the relationship between them. Honeycomb or foam have been classified as traditional core materials, to whom thin face sheets are bound for sandwich constructions. However, to decrease the damage, traditional core materials have been reinforced with nano sized fillers such as solid nano particles [1-3], nanoclays [4-9] and nano fibers [1;3].

However, due to the ease of processing, enhanced thermal-mechanical properties, wide availability and low cost, nanoclays have been found to be the ideal filler for reinforcement of polyurethane (PU) foams. Hosur et al. [10;11] and Njuguna et al. [7;12] showed that by adding a small amount of nanoclay as filler , major improvements in foam failure strength and energy absorption could be achieved. Building up on these previous studies [5-7], the montmorillonite used in this study has been modified with a quaternary ammonium salt before integration in the PU matrix, as reported in the literature this could increase the probability of an exfoliated structure [13-15].

Nano filled sandwich structures were then fabricated and tested on energy absorption capacity during low-velocity impact and quasi static compression. Further, new light weight, glass fiber reinforced thermoplast i.e. polyamide (PA6) and polypropylene (PP), face sheets have been utilized to increase weight reduction for potential applications, such as aircraft, ships, ballistic vests, and helmets to racing and high-end sports cars, providing structural stiffness and crash-energy management.

2. EXPERIMENTAL

2.1. Synthesis of nanoclay filled polyurethane foams. The nanoclay (OMMT) was acquired from LAVIOSA CHIMICA MINERARIA S.p.A., Italy under the trade name Dellite® 43B.

The preparation of the nano filled polyurethane foams consisted of three steps;

In the first step, polyol (Rokopol RF551®, PCC Rokita S.A., Poland) was stirred with the powdered OMMT. Rokopol RF551® was chosen as it is a general purpose sorbitol based polyether polyol recommended for the production of rigid polyurethane, which features low viscosity (4000 mPas), medium functionality and low reactivity and forms foams with excellent flow properties and good mechanical properties.

Then the catalyst (Polycat9®, Air Products and Chemicals, Inc., UK), water and surfactant (SR-321, Union Carbide, Marietta, GA) were added in order to prepare the polyol premix (component A). Polycat9® catalyst was chosen as it is a low odor tertiary amine that provides a balanced promotion of the urethane and urea reactions in flexible and rigid foam applications.

In the next step n-pentane as a physical blowing agent was added to component A. The disocyanate compound was polyphenyl-polymethylene-polyisocyanate (polymeric MDI) with an average functionality of 2.6-2.7 acquired from Borsodchem Polska Sp. z o.o. under the trade name ONGRONAT® 2100. This was added to component A and the mixture was stirred for 10 s with an overhead stirrer. Finally, the prepared mixtures were dropped into a mold. All the experiments were performed at ambient temperature of ca. 20°C.

2.2. Fabrication of face sheet panels. Glass fiber reinforced polyamide (MM-PA I 1F30, MACOMASS Verkaufs AG, Germany) and polypropylene (MM-PP-BI24, MACOMASS Verkaufs AG, Germany) were utilized as face sheet materials.

From this granulates, plates of 160x160x4 mm^3 were injection moulded and used as face sheets for sandwich fabrication. Fibre reinforced plates were prepared according to ISO 1268-10:2005(E). This standard specifies the general principles to be followed while injection moulding test specimens and promote uniformity in describing the main parameters of the moulding process and also to establish uniform practice in reporting moulding conditions. Interested readers on detailled understanding of polymer processing conditionsand parameters are refered to excellent works in the literature [16-18].Table 1 shows the injection moulding

parameters for plates on a Ferromatik K110 moulding machine with a closing pressure of 1100kN.

Table 1 Injection moulding parameters for face sheet manufacturing

2.3. Fabrication of sandwich panels. The face sheets were cleaned with ethanol prior application of the adhesive (DP8005 2 Part EPX Acrylic Adhesive, 3M). The adhesive was evenly distributed on the cleaned face sheet surface and pressed against the foam core, perpendicular to foam growth direction. With help of clamps the sandwich was fixed and let to cure for 12h. The dimensions of the final sandwich structures were; height 38mm, width 60mm and depth 60mm.

2.4. Foam characterization. The synthesized OMMT reinforced foam, intended as core materials were analyzed by means of Fourier transform infrared spectroscopy (FTIR), X-ray Diffraction (XRD), and thermogravimetric analysis (TGA).

The FTIR analysis of foamed materials was done using a BIORAD FTS-165 spectrometer.

XRD experiments were carried out on a Philips X-Pert diffractometer, with a graphite monochromator placed in front of the detector.

Thermogravimetric analysis was performed on a Netzsch TG 209 thermal analyzer, operating in a dynamic mode at a heating rate of 10 K/min. The conditions were: sample weight; 5 mg, atmosphere - argon, open Al_2O_3 pan.

Optical microscopy analyses were performed using a PZO optical microscope equipped with vision track. To analyse the cell size and geometry, Aphelion software was used. FT-IR spectra of the prepared foams were recorded using a BIORAD FTS 165 spectrometer, operating in the spectral range of 4000-400 cm^{-1}. Nanofoams were sliced by a rotary microtom (Leica, Microsystems Ltd.) and pressed against spectral potassium bromide grade.

2.5. Quasi-static compression testing. The sandwich panel were tested under quasi-static loading for subsequent comparison with results from impact loading. Quasi-static compression tests of the sandwich structures were conducted using an Instron 5500R universal testing machine. In both cases, the sandwich panel was simply supported on rollers

along two parallel edges. An indenter with a spherical surface of 10 mm radius introduced load at the centre of the panel. The deflection of the sandwich plate at the load point was recorded by the stroke of the Instron servo-hydraulic machine 100 kN load cell and the displacement was measured using a built in cross head displacement sensor. The displacement of the bottom face- sheet directly below the load point was recorded with a displacement transducer. The plate was loaded at a low rate until the first indication of damage initiation and then carefully unloaded. During the test the data was collected every 0.5 s, up to the maximum displacement of 24 mm.

Five specimens of each material system were tested, in foam growth direction, at cross head speed of 1 mm/min and an initial load of 20 kN. Compressive properties of the tested sandwich panels have been calculated according to BS ISO 844:2004. Compressive strength, with corresponding relative deformation was calculated. Additionally, compressive stresses at 10% relative deformation were calculated as the material yielded before completion of the test but still resist an increasing force.

2.6. Low-energy impact testing.

All the low impact tests were conducted using an instrumented falling weight impact device (drop tower). The device was equipped with data acquisition system to acquire force versus time data. Using this machine, impact energy and velocity can be varied by changing the mass and height of the dropping weight. The velocity of the falling drop mass is measured just before it strikes the specimen. It is also fitted with pneumatic rebound brake, which prevents multiple impacts on the specimen. During the testing, the specimen is held in the fixture placed at the bottom of the drop tower which provided a clamped circular support span (Figure 1) similar to quasi-static tests but using new set of specimens. The weight of cross-head is maintained at a specific value and it is guided through two frictionless guide columns. The impactor end of the drop mass is fitted with an instrumented tup with a hemispherical end having a capacity to record the transient response of the specimens. To carry out the impact tests, sandwich composite samples (60 mm × 60 mm x 38 mm) were placed between the clamps and the height was adjusted depending on the desired energy level. Two impactors were utilized, at (70 mm diameter) for surface load impact and a hemispherical tip (15 mm diameter) for localized point load impact. The energy level was kept at 15J for all impacts and the tests were repeated five times in each case. The transient force signal obtained during the

test was measured using a piezo-electric load cell located above the impactor tip and was routed through an amplifier and logged against a time-base.

3. RESULTS AND DISCUSSION

3.1. Morphology. The cell structure of the synthesized foams can be found in Figure 1 and Figure 2. Due to the anisotropic structural properties of the materials, which are a result from the forced growth of the foam, the materials were characterized in parallel and perpendicular directions. Mean area and number of cells in the OMMT-modified polyurethane systems were determined and can be found in Table 2. Further an apparent density of 40.7, 38.7, 40, 39.6 and 39.2 kg/m^3 was measured for the 0, 2.5, 5, 7.5 and 10 wt.% filled foams.

Figure 1 Cell structure of modified PU/OMMT foamed materials parallel to the direction of foam's growth

Figure 2 Cell structure of modified PU/OMMT foamed materials perpendicular to the direction of foam's growth

The number of cells per square millimeter and their shape (the anisotropy index) is a critical parameter that strongly influences the thermal insulating properties of foamed materials [19]. As the number of cells increases, the coefficient of thermal conductivity decreases. Regarding the anisotropy index, with increasing values the heat flow decreases providing that the heat flow direction is perpendicular to cell height (the longer cell dimension). The foaming method affects the cell structure of foams, particularly the mould shape and dimensions. During the foaming process elongation of cells in the direction of foam growth is observed depending on type of mould.

An increase of anisotropy index in parallel direction to the foam growths could be found for the PU/nanoclay foam. It has to be noted that for the given amount of OMMT content the amount of modifier is already incorporated in the given value. The highest anisotropy index could be detected for the foams with 5 and 10 wt.% of OMMT loading. The incorporation of OMMT resulted in smaller number of cells with higher dimensions and higher anisotropy index for the parallel cross sections. In the case of perpendicular direction an increase content of number of cells with smaller dimensions was observed. The changes in the cellular structure of the materials obtained can be caused by the forced direction of foam growth, as PU foams are highly anisotropic materials.

The choice of foaming methods affects the foam-cell structure, particularly the mould shape and dimensions. Amount and distribution of nucleation agents are also crucial factors for obtaining foam cells with a controlled structure and uniform distribution [2;20]. The effect of nanoclay dispersion on the cells' structure has been studied in the literature [12-23]. It was shown that the exfoliated nanoclay filled polyurethane foams achieved a much higher nucleation rate than the intercalated nanocomposites, hence a more uniform cell distribution. Once the particles were better dispersed (at the same nominal particle concentration), the effective particle concentration was higher, and thus a more heterogeneous nucleation sites was obtained. Further, the effect of nanoclay on the cell size was studied by Okamoto et al. [21] who found that the cell size was reduced in the presence of nanoclay. The reduction of cells is caused by the increase of bubbles that start to concurrently nucleate, which cause less amount of gas available for bubble growth. Besides, the surface chemistry of the nanoclays has an effect on the nucleation efficiency in polymer/clay foamedt system [24].

Table 2 Structural properties of the PU/OMMT nanofoams

3.2. FTIR and WAXS analysis of PU modified with OMMT. The FTIR analysis of PU-based materials showed the formation of bands characteristic for polyurethane, and can be found in Figure 9. The following bands were identified from FTIR measurements; absorption bands at 3345 cm^{-1}, due to the N-H stretching, and bands around 2946, 2911 and 2871 cm^{-1} due to the C-H stretching in $-CH_2-$ groups. The bands at 1717 and at 1507 cm^{-1} were connected with the stretching vibrations of C=O in urethane and allophanate groups (I amide

band) and to the deformation vibrations of N-H bond (II amide band), respectively. C-H stretching vibrations were reacted in the absorption band maximum at 1596 cm^{-1}. Another possible origin of that band is the deformation vibration of N-H in urethane group. The bands at 1412 cm^{-1} were known to origin from the carbonyl of urethane group forming a hydrogen bonding, allophanate and biureth bond. Bands at 1285, 1223 and 1071 cm^{-1} were due to the polyethers used as a polyol component. The FTIR analysis confirmed the formation of polyurethane in a presence of nanofiller. The band characteristic for montmorillonite was observed in a range of 1000-1100 cm^{-1} as a broadening of absorption band corresponding to ether bound in polyol compound (Figure 3 b).

Figure 1 FTIR spectrum of PU/OMMT nanocomposites a) full spectrum, b) 950-1300 cm^{-1}.

The nanoinduced foams were submitted to WAXD analysis in order to assess the structure of the polymeric material and possible regular arrangement of the organophilic montmorilonite. The diffraction patterns of the neat PU sample did not reveal any crystalline phases in the material. Figure 4 displays the diffractogram of neat PU foams and PU/OMMT nanocomposite with a diffraction angle 2θ between 3° and 60°. The structure of the PU and PU/OMMT foam specimen was completely amorphic. Since the raw materials were multifunctional, it is likely that a cross linked polymer was formed without ability to form polymer crystals. The lamellar arrangement of OMMT was maintained in the nanocomposite as evidenced by the diffraction peak at ca. 5.5°, which is assigned to the (001) lattice spacing of the nanoclay and can be seen in Figure 4 b.

The polyurethane is an amorphous polymer - the raw materials were multifunctional and in the polymerization process it is likely that a cross-linked network was formed without ability to form crystalline phase. The lamellar arrangement of OMMT was maintained in nanocomposite as evidenced by the diffraction peak at 4.75º. The peak maximum was shifted towards lower angles as compared to neat nanofiller, therefore an intercalated structure of PU/MMT nanocomposite can be postulated.

Figure 4 WAXD diffractogram of neat PU foams and nanoclay filled foams a) diffraction angle 2θ between 3° and 60° b) diffraction angle 2θ between 4° and 6.5°.

3.3. Thermal Stability. The results of the thermogravimetric analysis of modified PU can be found in Figure 5. The degradation of the nanoclay filled polyurethane foams run in one distinct stage with a maximum of mass loss around 345°C. The degradation process was only slightly incensed by organophilic montmorillonite by shifting the degradation by a few degrees towards higher temperatures. The shift of degradation towards higher temperatures was caused by the suppression of the molecular mobility of polymer chains by the OMMT layers (Figure 5b). As no thermal stabilizers were used, the following effects may have influence the nature and extent of the thermal decomposition; (1) specific intermolecular interactions via hydrogen bonding, (2) crystallinity, and (3) the presence of chemical cross-linking. For instance, Wang et al. [25] postulated that the degree of phase separation and specific interactions play a major role in the decomposition of polyurethanes. The extent of inter-urethane hydrogen bonding, arising from the incomplete phase separation between the soft and hard segments, was found to influence the thermal stability of PU's under investigation. In a different work, Ferguson et al. [26] has shown evidence for the mutual stabilization effect of soft- and hard-phase based on a protection function of soft segments through different functional groups and hydrogen bonding. Integrated absorbance data shows that the hydrogen-bonding behavior in polyurethanes is insensitive to crystalline transitions within the hard segment microdomains, but that it does reflect the morphological transitions in a block copolymer that are associated with intersegmental mixing [27].

Figure 2 TG and DTG curves of PU/OMMT composites

3.4. Quasi-static compression behavior. The stress-strain relationship for the sandwich panels can be found in Figure 6 and the compression properties are provided in Table 3. For all manufactured sandwiches, a decrease in compressive properties was measured. Compressive strength and stress (at 10% relative deformation) decreased with increasing filler loading. A variation in compressive stress, for the different face sheets could be identified for lowered deformations. However, once 10% relative deformation was reached the sandwiches with different face sheets resulted in the same compressive stresses. Nevertheless, an increase in compressive modulus could be achieved for the PA6 face sheet sandwiches. As explained in section 3.2., there was neither phase separation nor agglomeration of nanoclay in the foam

core due to proper distribution of OMMT in the polyol component. As described in the experimental section, low viscosity polyol was efficiently stirred with the powdered OMMT to produce homogeneous suspension applied in next synthesis steps. The resultant PU/OMMT material was an intercalated nanocomposite as revealed by WAXD analysis - the 2θ peak maximum was shifted towards lower angles as compared to neat nanofiller. As such, it appears that there is a critical load of nanoreinforcements above which the mechanical properties of PU foams are not considerably get changed. This is illustrated by the plateau stress as a function of the volume fraction of nanoclay in the stress-strain curves.

Figure 6 Stress-strain relationship for sandwiches panels

Table 3 Compression properties

Figure 7 shows the dependency of energy absorption during compression in relation to the filler loading of the sandwich core foam. Energy absorption increases with higher filler loadings respectively. An increase of up to 40% could be measured for both PP and PA face sheets, for the 10 wt.% nanoclay loaded foam.

Figure 7 Energy absorption vs. composite loading

The decrease of compressive strength, stress and energy absorption properties of the 5 wt.% OMMT loaded sandwiches can be explained by the high number of cells which result in the smallest average cell surface area. It follows polyurethane, like many synthetic polymers are produced by reacting monomers in a reaction vessel. In order to produce polyurethane, polyaddition process is performed. In this type of chemical polymerisation reaction, the monomers that are present contain reacting end groups. Specifically, a diisocyanate (OCN-R-NCO) is reacted with a diol (HO-R-OH). The first step of this reaction results in the chemical linking of the two molecules leaving a reactive alcohol (OH) on one side and a reactive

isocyanate (NCO) on the other. These groups react further with other monomers to form a larger, longer macromolecule. This is a rapid process which yields high molecular weight polyurethane materials even at room temperature.

According to Cao et al. [28], the overall compressive performance of PU nanocomposite foams depends on the competition between the positive effects of clay on polymer reinforcement and foam morphology, and the negative effects on H-bond formation and network structure. It is well known that the strength and the modulus of PU foams are dependent on the H-bond formation among urethane groups. PU molecules can be grafted onto the clay surface through the reaction between -NCO groups on the clay, so that the clay possibly interferes with the H-bond formation in the PU. This caused a negative effect on the properties of the PU nanocomposite foams. Similar results were reported by Harikrishnan et al. [29] as no significant increase in the compressive strength was found with the addition of clay. They stated that with higher clay loading, compressive strength showed a decreasing trend which was caused by the weakening of foam structure due to formation of large voids. Kim et al. [30] explained the decrease of compression strength of their nanoclay reinforced PU foams with the decrease of density of the foams with increasing clay content.

3.5. Low energy impact behavior. Manufactured sandwich panels were subjected to low energy impact test. Samples of each set were tested at an energy level of 15J with a hemispherical and a flat striker. Transient data were collected for each sample, which included time, load, energy, velocity and deflection, and can be found in Table 4.

Table 4 Impact performance properties

The increase of absorbed energy could be calculated, respectively. Energy absorption in any material under impact loading is mainly a caused due elastic deformation (in an initial stage) [12]. Some of the energy can additionally be absorbed through friction. Once the energy level exceed the level required for maximum elastic deformation, the structure dissipates the excess energy in form of plastic deformation or through various damage mechanisms. The difference in energy absorption mechanism for nanoreinforced foams can be seen in Figure 8.
Neat foams showed signs of plastic deformation while the nano filled foam clearly showed signs of fracture damage. With increased percentage of filler loading, the degree of fracture

increased as well. Since the characteristics for this fracture mode were, that axial cracks were being initiated at the early stage of the impact event and stopped quickly after the formation due to the geometrical constrains of the cell morpology. Therefore, the size of the generated cracks and debris, hence damage, was significantly smaller than the cracks and debris size observed for elastic deformation of the neat PU foams. In general the degree of deformation decreased and the degree of fracture increased with increasing filler loads. The increase of brittleness in relation to OMMT filling was also observed in the literature by Yang et al. [31] and Zoukrami et al. [32]. Therefore, this led to the conclusion that nano reinforcement leads to changes in the energy absorption mechanism of the material studied. Further, with increasing clay content the core material stared to get more brittle [10;11]. The brittleness of the material causes larger cracks and fragmentation, reducing the energy absorption capabilities of the material [33,34].

Figure 3 Typical damage on the sandwich panels after 15J point impact. The sandwich core damage increased with filler wt% loading with the 10 wt.% displaying maximum damage for sandwich composites studied

PA6 face sheets absorbed more impact energies and for their sandwich structures a higher peak load was recorded, compared to the PP sandwich structures. The improvement in energy absorption was between 66-92% for PP face sheet sandwiches and 23-34% for the PA6 face sheet sandwiches, under point load. Load-deflection graphs can be found in Figure 9. The specimen did not show any perforation during the impact, hence the impactor renounced and the force returned to zero after impact. However, due to the high level of noises, the graphs got incomprehensive (Figure 9e). Therefore, Figure 9 only demonstrates the behaviour of the specimen when subjected to the load.

While the maximal peak load for all impacts could be found for the neat PP/PU and PA/PU sandwiches, reinforcement with nanoclay caused increased deflection. The deflection at peak load and the maximum deflection are qualitative indication of the stiffness of the material. The deflection at peak load varied between ±1mm for the sandwiches subjected to point impact, an increase of 10-12 mm was measured for the surface impacted sandwiches. There were no visible cracking or deformation on the surface of the reactive foam cores along the length of the structures. Compliant specimen took more time to complete the impact event and

also showed increased deflection, which in the current case the nanoclay filled polyurethane foams sandwiches shows more tailoring potential for crashworthiness applications.
This results are in conflict with results obtained earlier by Hosur et al. [10;11] and Njuguna et al. [5-7] who reported an increase of peak load for nanoclay filled foams. Nevertheless, it should be noted that the morphology of the PU/OMMT nano foams utilized in [5-7], was very different from the one used in the present study. The utilized foams had twice the number of cells in perpendicular and parallel direction, which resulted that the average cell surface area was half the area detected in this study.

Figure 9 Load-deflection graphs for point load and surface impact. It should be noted that all the specimens reported (a-d) did not show any perforation during the impact and hence the force returned to zero for each test carried out as shown on in (e).

4. CONCLUSIONS

Sandwich panels were fabricated with nanoclay filled polyurethane foams cores and glass fiber reinforced polyamide and polypropylene face sheets. Pore structure of the different loaded foams was found to be rather similar in parallel and perpendicular direction to the foam growing direction. The degradation rate of the PU foams was slightly enhanced by the presence of OMMT. Further, the addition of nanoclay increased the energy absorption capacity during compression and low energy impact tests. However, lower values for compressive strength and peak load were recorded. The usage of different face sheets has showed little difference for the quasi static compression tests. However, once the sandwiches were subjected to low energy impact tests the PA6 face sheet shown superiority over the PP face sheet. Although a significant amount of work has already been done on various aspects of PU nanofoam for sandwich composites much research still remains in order to understand the complex structure-property relationships.

ACKNOWLEDGEMENTS

This work was funded by the European Commission Framework 7 Project - CP-FP7 Project Reference No. 228536 - 2 titled 'Nanomaterials-related environmental pollution and health hazards throughout their life-cycle' (NEPHH). Additionally, the authors would like to thank the EPSRC Equipment Pool for the utilisation of the high speed camera.

REFERENCES

[1] Bhuiyan M. A., Hosur M. V., and Jeelani S. Low-velocity impact response of sandwich composites with nanophased foam core and biaxial formula not shown braided face sheets. Composites Part B, 40:561;571, 2009.

[2] Park C. B., Behravesh A. H., and Venter R. D. A strategy for the suppression of cell coalescence in the extrusion of microcellular high-impact polystyrene foams. ACS Symposium Series., 669:115, 1997.

[3] Saha M. C., Kabir E., and Jeelani S. Study of debond fracture toughness of sandwich composites with nanophased core. Materials Letters, 62:567-570, 2008.

[4] S. Sachse, F. Silva, K. Pielichowski, A. Leszczynska, J. Njuguna, Compression strength and low-velocity impact performance of nanocored sandwich composites, Mechanics of Nano, Micro and Macro Composite Structures, Politecnico di Torino,18-20 June 2012.

[5] Njuguna J., Pena I., Zhu H., Rocks S. A, Blazquez M., and Desai S. A. Opportunities and environmental health challenges facing integration of polymer nanocomposites technologies for automotive applications. International Journal of Polymers and Technologies, 1(1-3):113-122, 2009.

[6] Njuguna J., Pielichowski K., and Desai S. Nanofiller -reinforced polymer nanocomposites. Polymers for Advanced Technologies, 19(8):947-959, 2008.

[7] Njuguna J., Michalowski S., Pielichowski K., Kayvantash K., and Walton A. C. Fabrication, characterization and low-velocity impact testing of hybrid sandwich composites with polyurethane/layered silicate foam cores. Polymer Composites, 32(1):6-13, 2011.

[8] Gupta N. and Maharsia R. Enhancement of energy absorption in syntactic foams by nanoclay incorporation for sandwich core applications. Applied Composite Materials, 12:247;261, 2005. 10.1007/s10443-005-1130-6.

[9] Tomy Widya and Christopher W. Macosko. Nanoclay modified rigid polyurethane foam. Journal of Macromolecular Science, Part B, 44(6):897-908, 2005.

[10] Hosur M. V., Mohammed A. A., Zainuddin S., and Jeelani S. Impact performance of nanophased foam core sandwich composites. Materials Science and Engineering: A, 498:100 ; 109, 2008.

[11] Hosur M. V., Mohammed A. A., Zainuddin S., and Jeelani S. Processing of nanoclay filled sandwich composites and their response to low-velocity impact loading. Composite Structures, 82:101-116, 2008.

[12] Njuguna J. The application of energy absorbing structures on side impact protection systems. International Journal of Computer Applications in Technology, 40:280-287, 2011.

[13] Park J. H. and S. C. Jana. Mechanism of exfoliation of nanoclay particles in epox -clay nanocomposites. Macromolecules, 36(8):2758-2768, 2003.

[14] Park J. and Jana S. C. Effect of plasticization of epoxy networks by organic modifier on exfoliation of nanoclay. Macromolecules, 36(22):8391-8397, 2003.

[15] Park J. and Sadhan C. J. Adverse effects of thermal dissociation of alkyl ammonium ions on nanoclay exfoliation in epox -clay systems. Polymer, 45:7673-7679, 2004.

[16] Cheremisinoff, N. P., and Cheremisinoff, P. N. (Eds.). (1996). Handbook of applied polymer processing technology (Vol. 31). CRC Press.

[17] Harper, C. A. (2006). Handbook of plastic processes. Wiley, New York 2006,

[18] Bryce, D. M. (1996). Plastic Injection Molding: Manufacturing Process Fundamentals (Vol. 1). SME, SME, Dearborn 1996.

[19] A. Prociak, Cell structure – thermal conductivity relationships of polyurethane and polystyrene foams. Fifth International Conference on Foam Processing & Technology, FOAMS 2006, Chicago, USA, Conference Proceedings on CD, 2006.

[20] Lee L. J., Zeng C., Cao X., Han X., Shen J., and Xu G. Polymer nanocomposite foams. Composites Science and Technology, 65:2344-2363, 2005.

[21] Zeng C. Polymer nanocomposites: synthesis, structure and processing. PhD thesis, The Ohio State University, 2003.

[22] Zeng C., Lee L. J. Han X., Koelling K. W., and Tomasko D. L. Polymer/clay nanocomposite foams prepared using carbon dioxide. Adv Mater, 15:1743, 2003.

[23] Han X., Zeng C., Lee L. J., Koelling K. W., and Tomasko D. L. Extrusion of polystyrene nanocomposite foams with supercritical carbon dioxide. Polymer Engineering and Science, 43(6):12611275, 2003.

[24] Okamoto M., Nam P. H., Maiti P., Kotaka T., Nakayama T., Takada M., Ohshima M., Usuki A., Hasegawa N., and Okamoto H. Biaxial ow-induced alignment of silicate layers in polypropylene/clay nanocomposite foam. Nano Letters, 1(9):503-505, 2001.

[25] Wang T. L., Hsieh T. H., Effect of Polyol Structure and Molecular Weight on the Thermal Stability of Segmented Poly(urethaneureas), Polymer Degradation and Stability, 55, 95, 1997.

[26] Ferguson J., Petrovic, Z., Thermal Stability of Segmented Polyurethanes, European Polymer Journal, 12, 177, 1976

[27] Koberstein J.T., Gancarz, I., Clarke, T. C., The effects of morphological transitions on hydrogen bonding in polyurethanes: Preliminary results of simultaneous DSC-FTIR experiments, Journal of Polymer Science Part B: Polymer Physics, 24 (1986) 2487–2498

[28] Cao X., Lee L. J., Widya T., and Macosko C. Polyurethane/clay nanocomposites foams: processing, structure and properties. Polymer, 46(3):775-783,2005.

[29] Harikrishnan G., Umasankar Patro T., and Khakhar D. V. Polyurethane foam- clay nanocomposites: Nanoclays as cell openers. Industrial & Engineering Chemistry Research, 45(21):7126-7134, 2006.

[30] Kim S. H., Lee M. C., Kim H. D., Park H. C., Jeong H. M., Yoon K. S., and Kim B. K. Nanoclay reinforced rigid polyurethane foams. Journal of Applied Polymer Science, 117(4):1992-1997, 2010.

[31] Yang F., Ou Y., and Yu Z. Polyamide 6/silica nanocomposites prepared by in situ polymerization. Journal of Applied Polymer Science, 69(2):355-361, 1998.

[32] Zoukrami F., Haddaoui N., Vanzeveren C., Sclavons M., and Devaux J. Effect of compatibilizer on the dispersion of untreated silica in a polypropylene matrix. Polymer International, 57(5):756-763, 2008.

[33] Sachse, S., Michałowski S., Leszczyńska, A., Pielichowski, K., Zhu, H.,The release of nanofillers from polymer matrix: Case studies on polypropylene, polyamide and polyurethane nanoreinforced composites, Nanoproduct Review Journal, 1(1); p.201303.

[34] Sachse, S., Gendre, L., Silva, F., Zhu, H., Leszczyńska, A., Pielichowski, K., Ermini V. and Njuguna, J. On nanoparticles release from polymer nanocomposites for applications in lightweight automotive components. Journal of Physics: Conference Series, 429(1): p. 012046,2013.

Figures and Tables

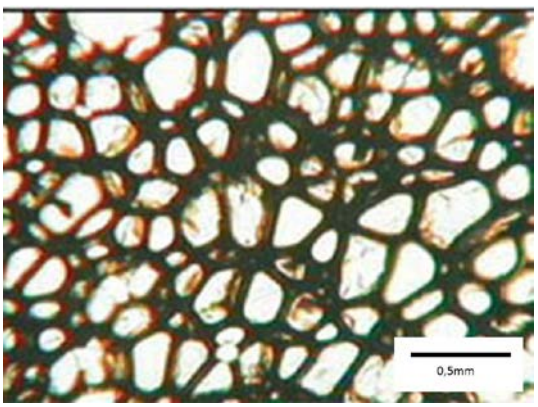

(a) 0 wt. %OMMT

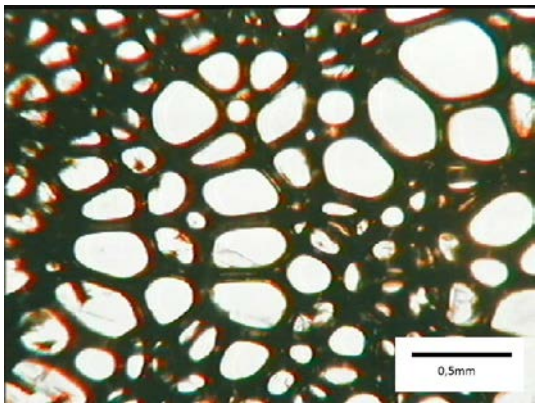

(b) 2.5 wt. %OMMT

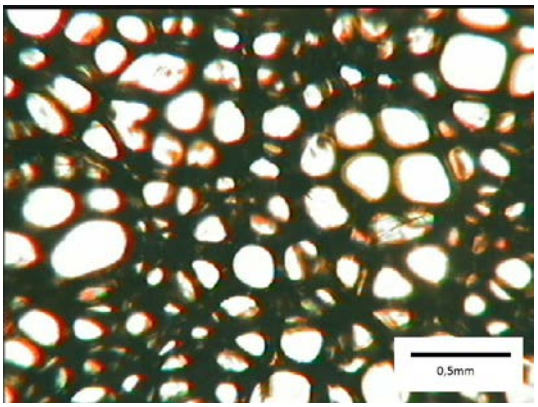

(c) 5 wt. %OMMT

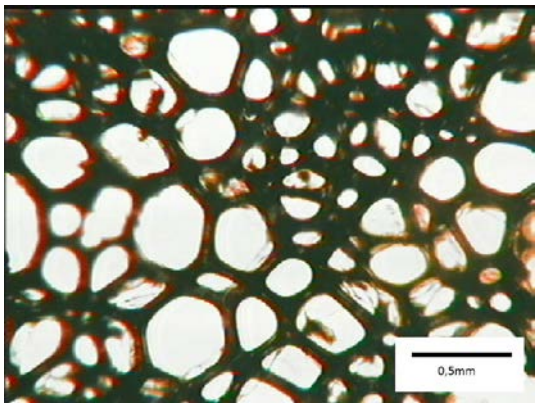

(d) 7.5 wt. %OMMT

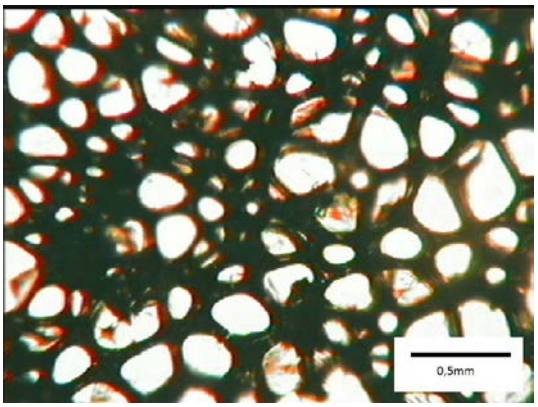

(e) 10 wt. %OMMT

Figure 1 Cell structure of modified PU/OMMT foamed materials parallel to the direction of foam's growth

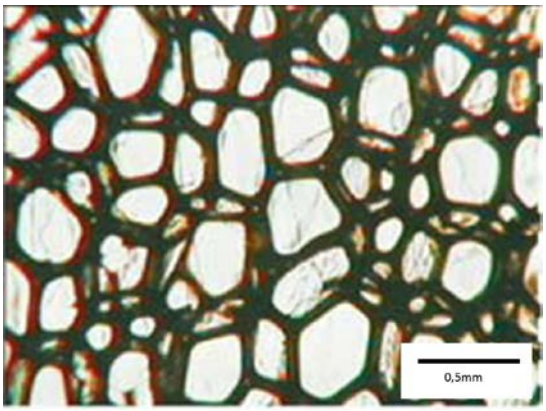

(a) 0 wt. %OMMT

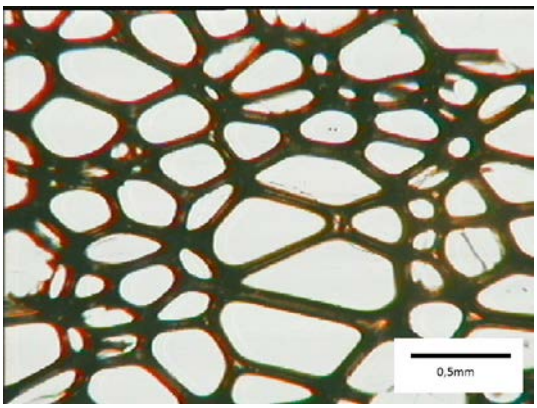

(b) 2.5 wt. %OMMT

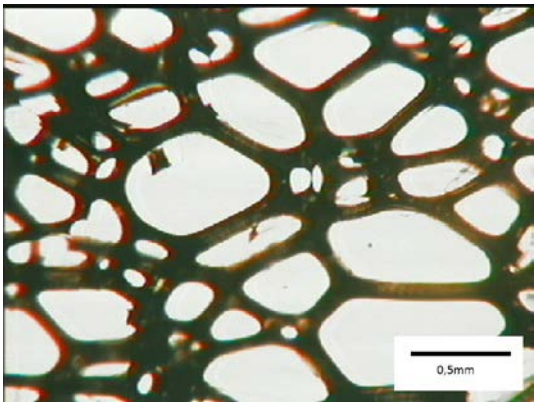

(c) 5 wt. %OMMT

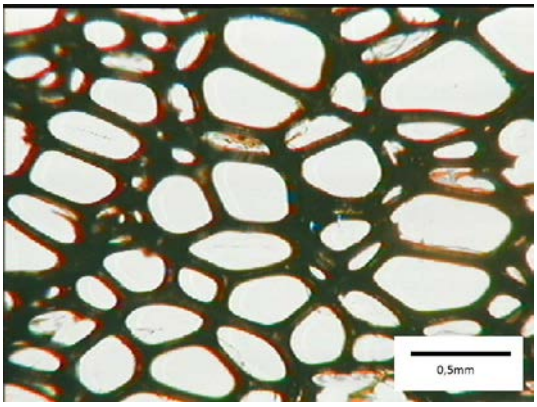

(d) 7.5 wt. %OMMT

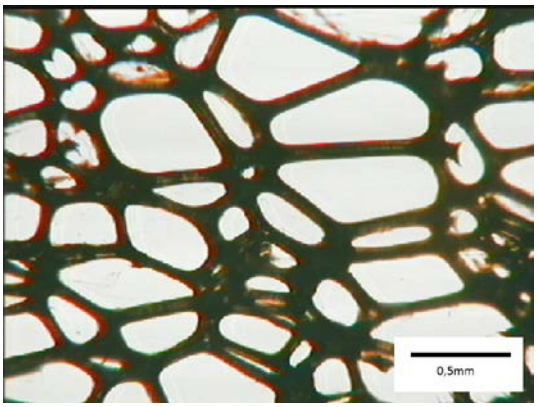

(e) 10 wt. %OMMT

Figure 2 Cell structure of modified PU/OMMT foamed materials perpendicular to the direction of foam's growth

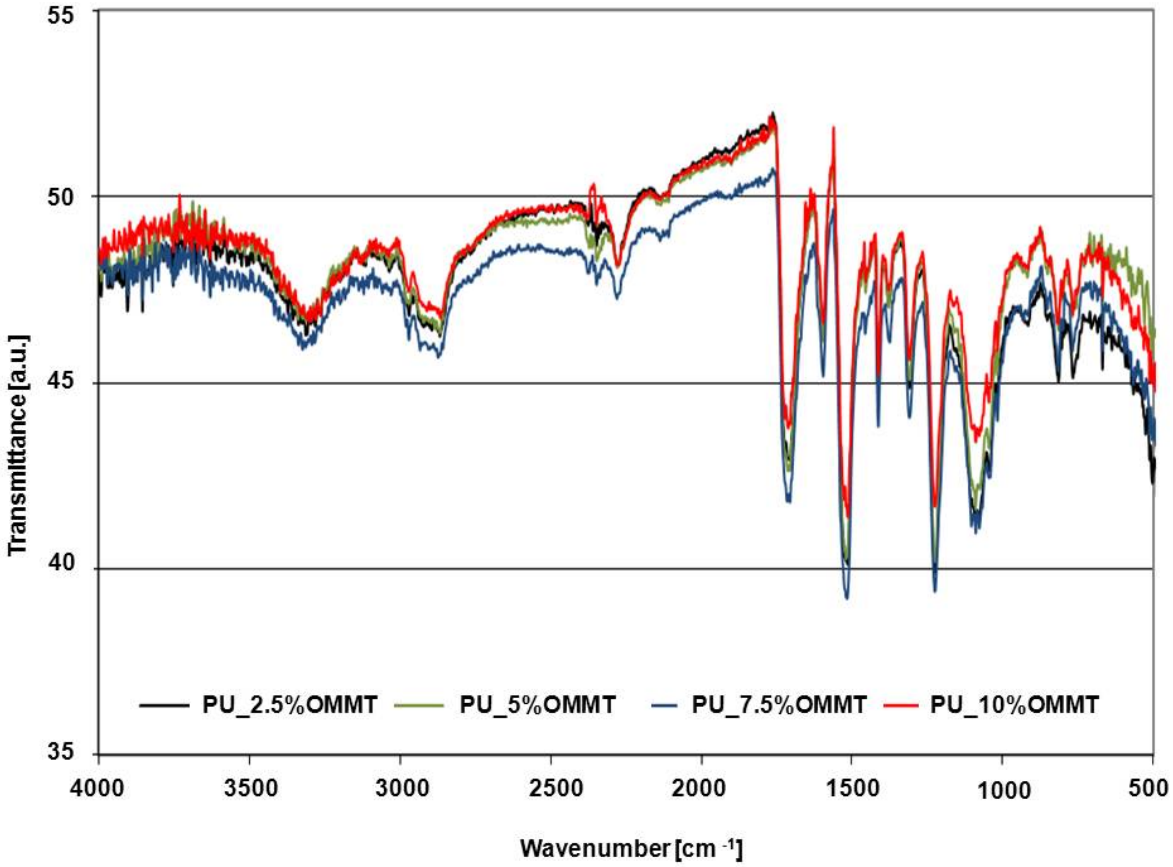

a) Full Spectrum

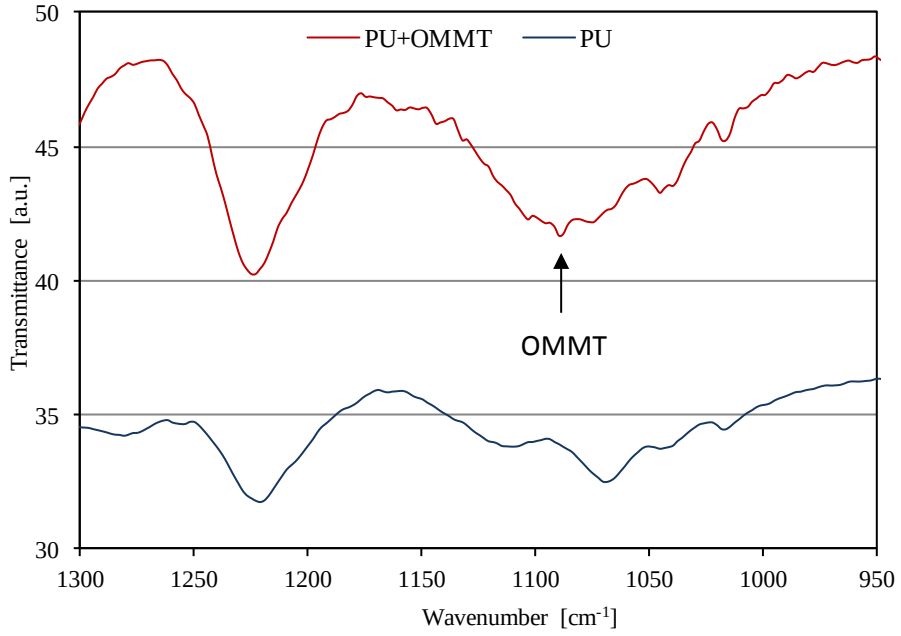

b) Spectra at 950-1300 cm^{-1}.

Figur e 3 FTIR spectrum of PU/OMMT nanocomposites a) full spectrum b) 950-1300 cm^{-1}.

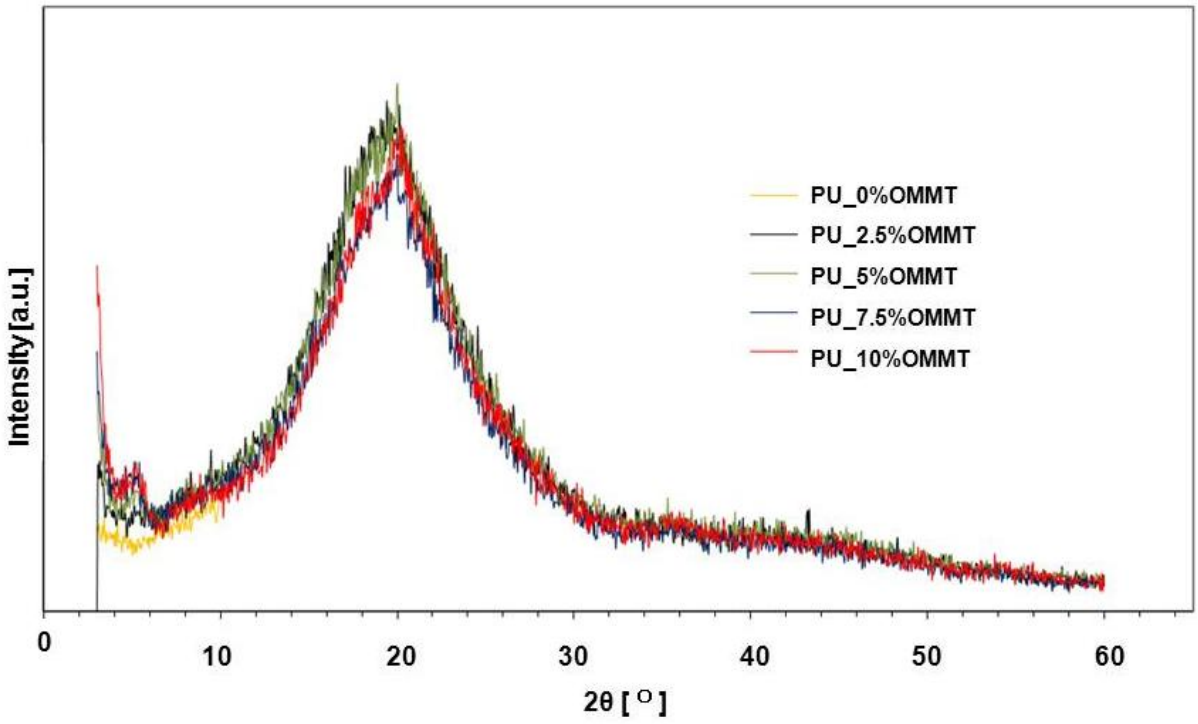

a) Diffraction angle 2 θ between 3 and 60°

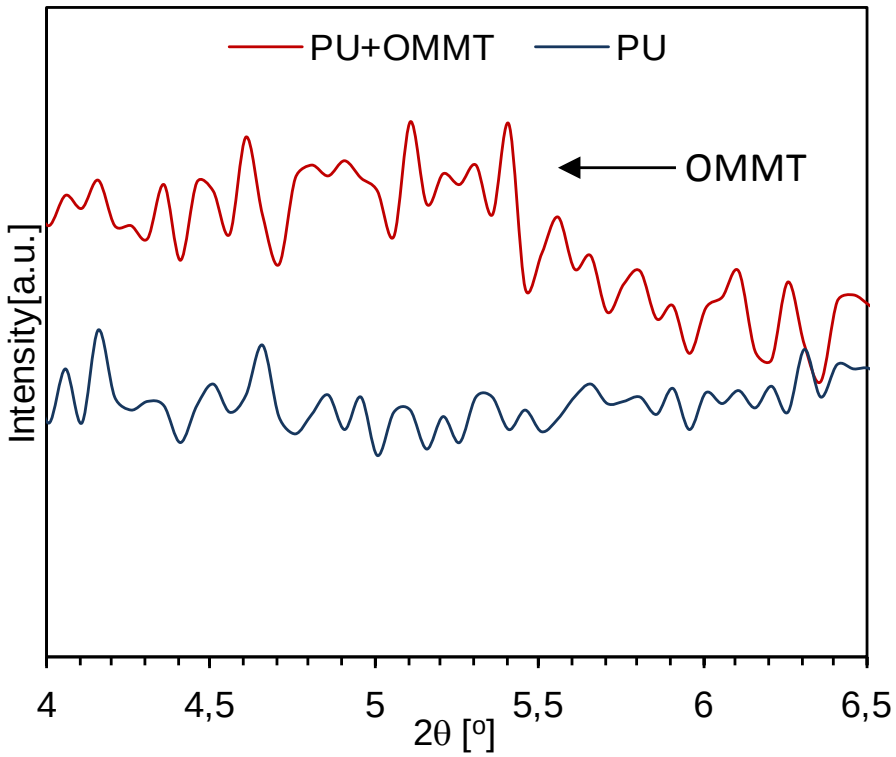

b) Diffraction angle 2 θ between 4 and 6.5°.

Figure 4 WAXD diffractogram of neat PU foams and nanoclay filled foams a) diffraction angle 2θ between 3° and 60° b) diffraction angle 2θ between 4° and 6.5°.

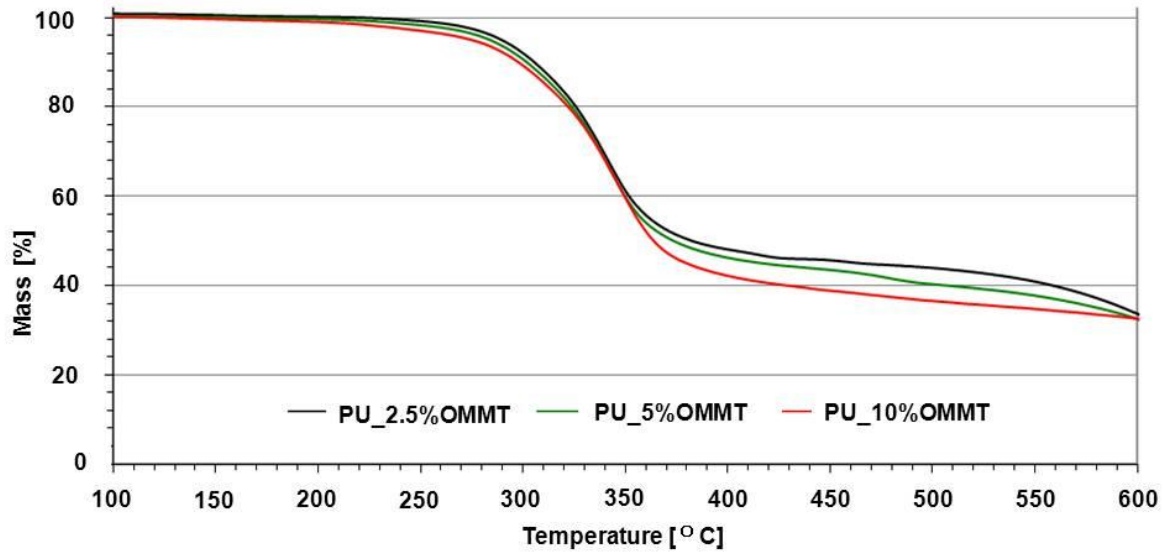

(a) TG

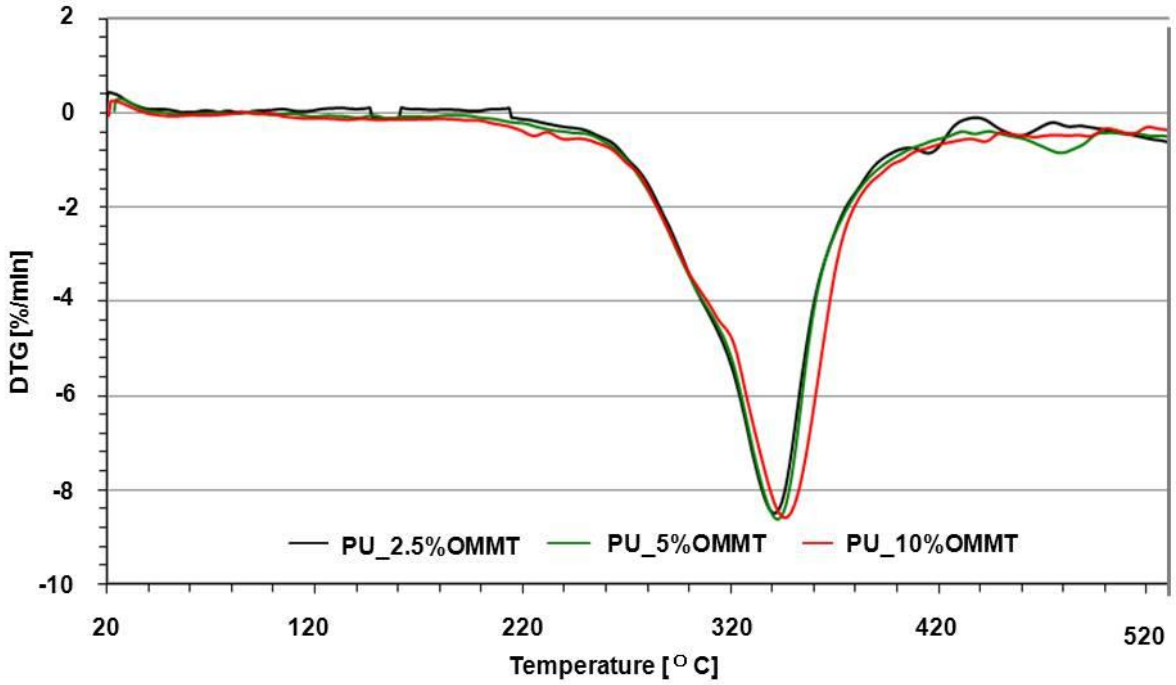

(b) DTG

Figure 5 TG and DTG curves of PU/OMMT composites

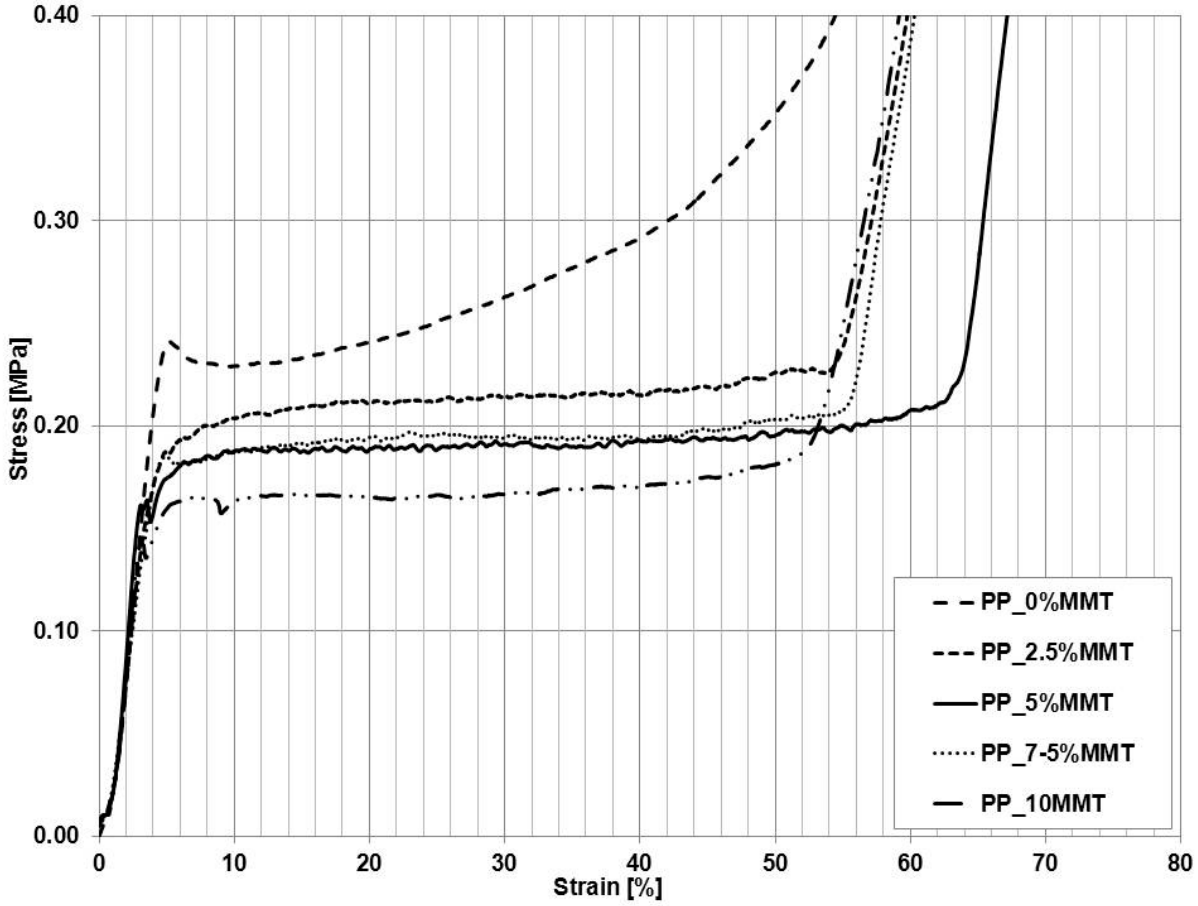

6(a) PP-PU/MMT sandwiches

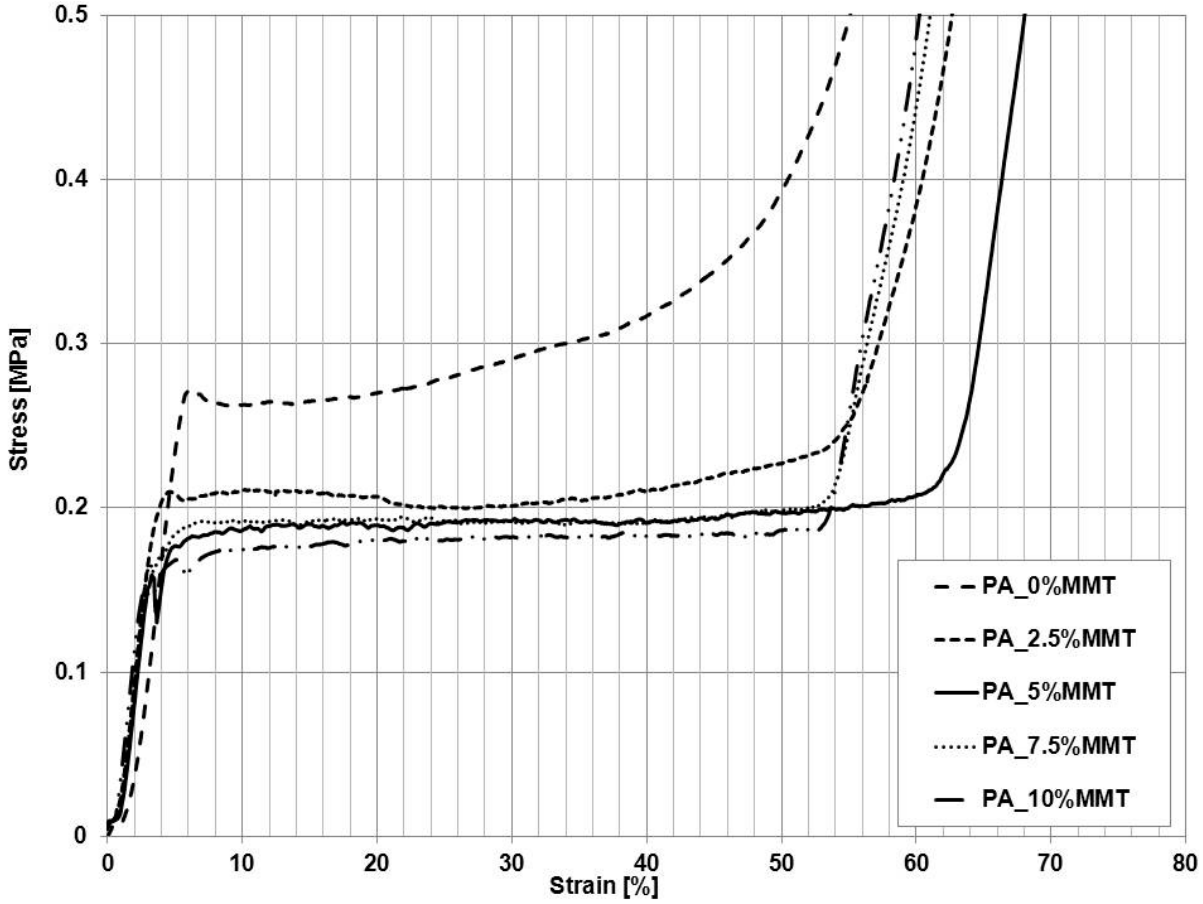

6(b) PA-PU/MMT sandwiches

Figure 6 Stress-strain relationship for sandwiches panels

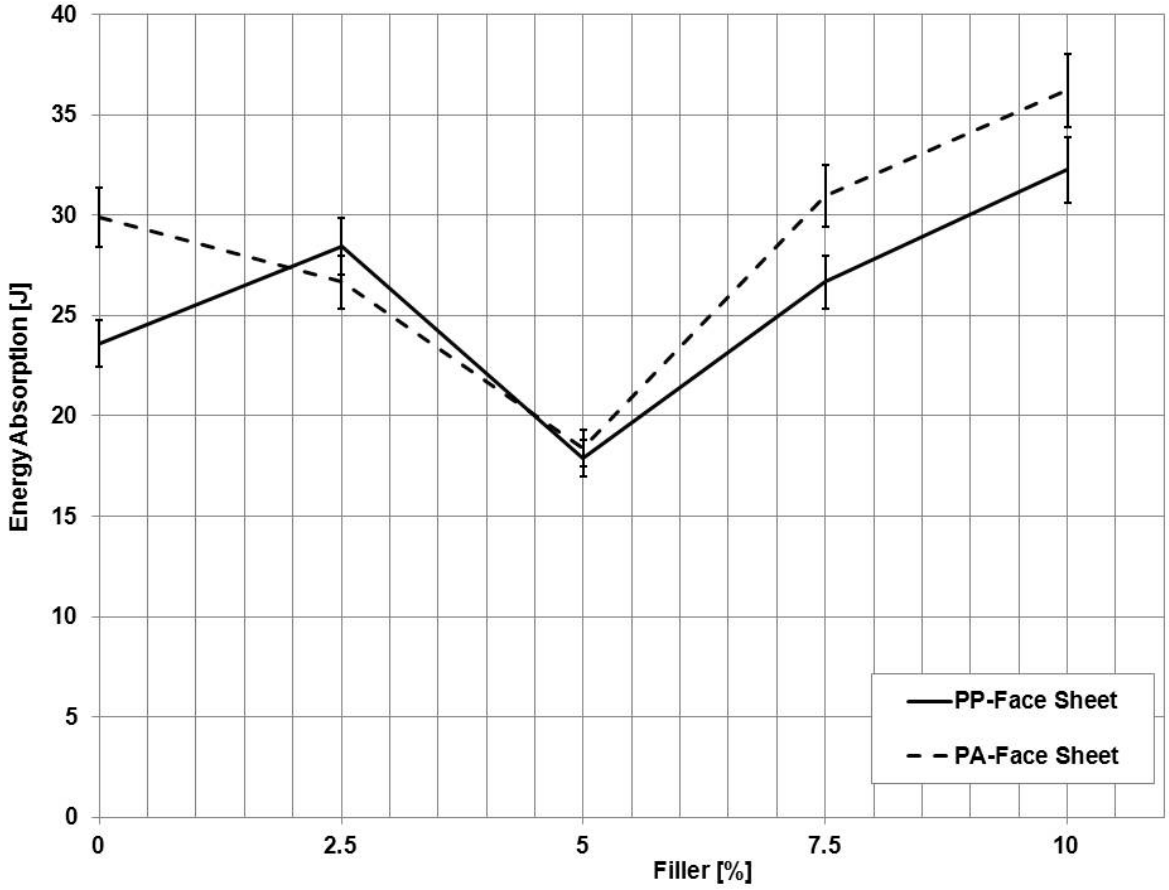

Figure 7 Strain energy against nanofiller loading wt.% for the composites studied

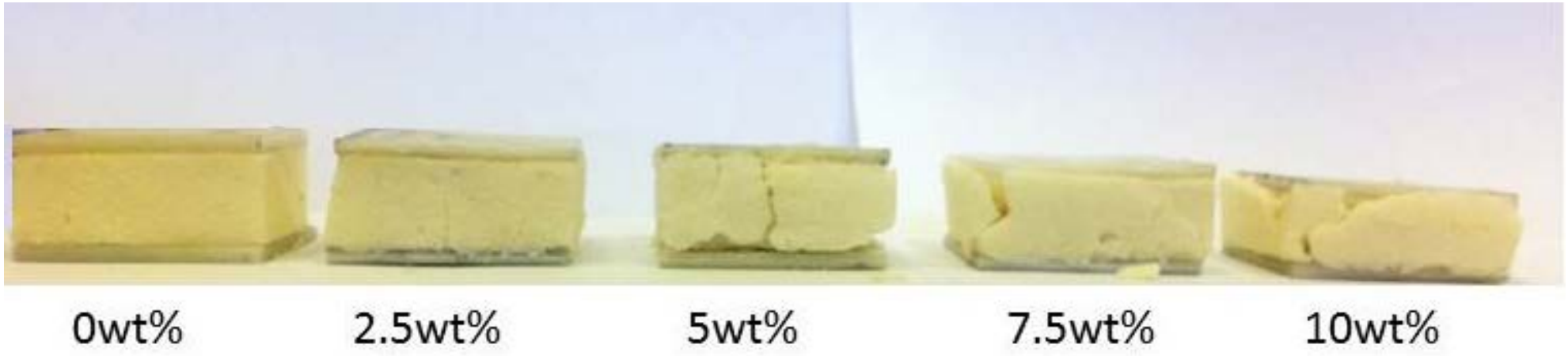

Figure 8 Typical damage on the sandwich panels after 15J point impact. The sandwich core damage increased with filler wt% loading with the 10 wt.% displaying maximum damage for sandwich composites studied

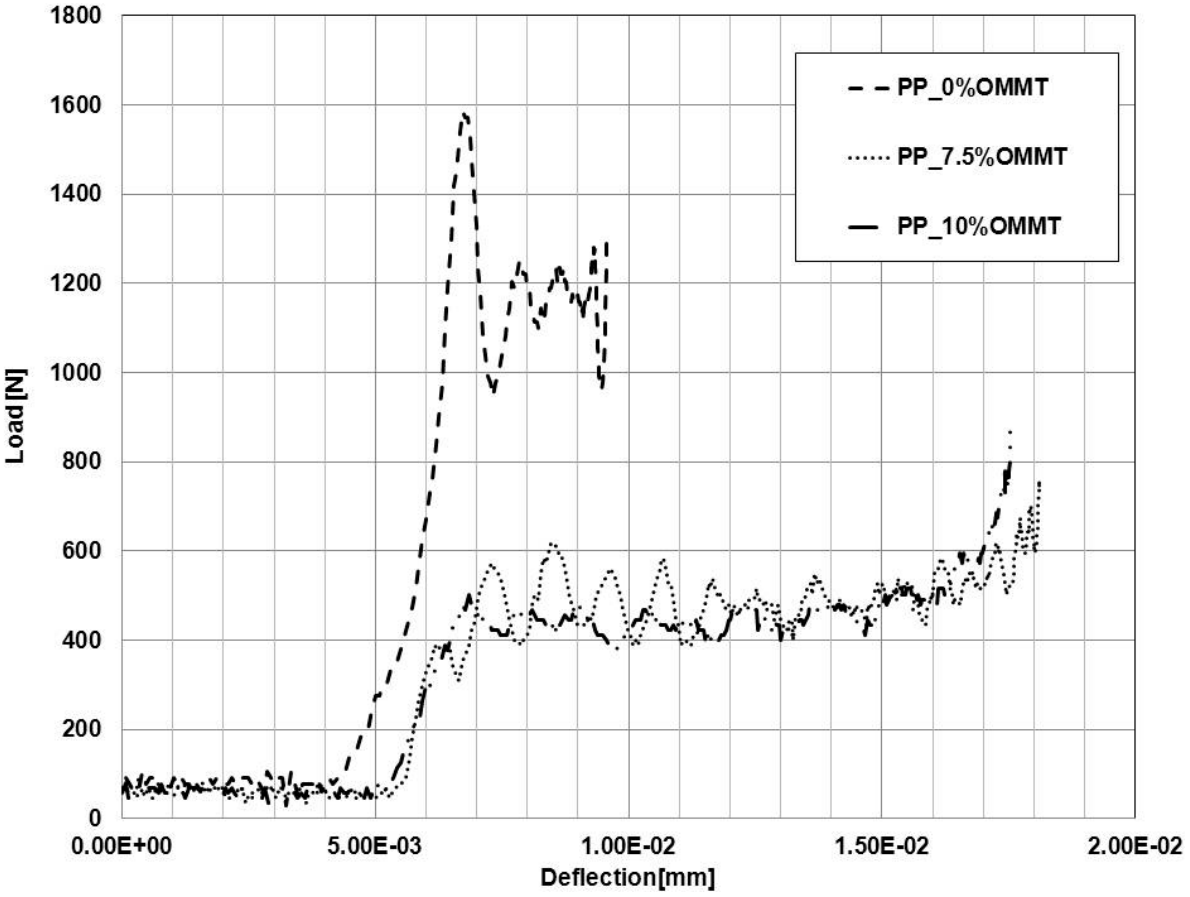

9(a) PP Surface Impact

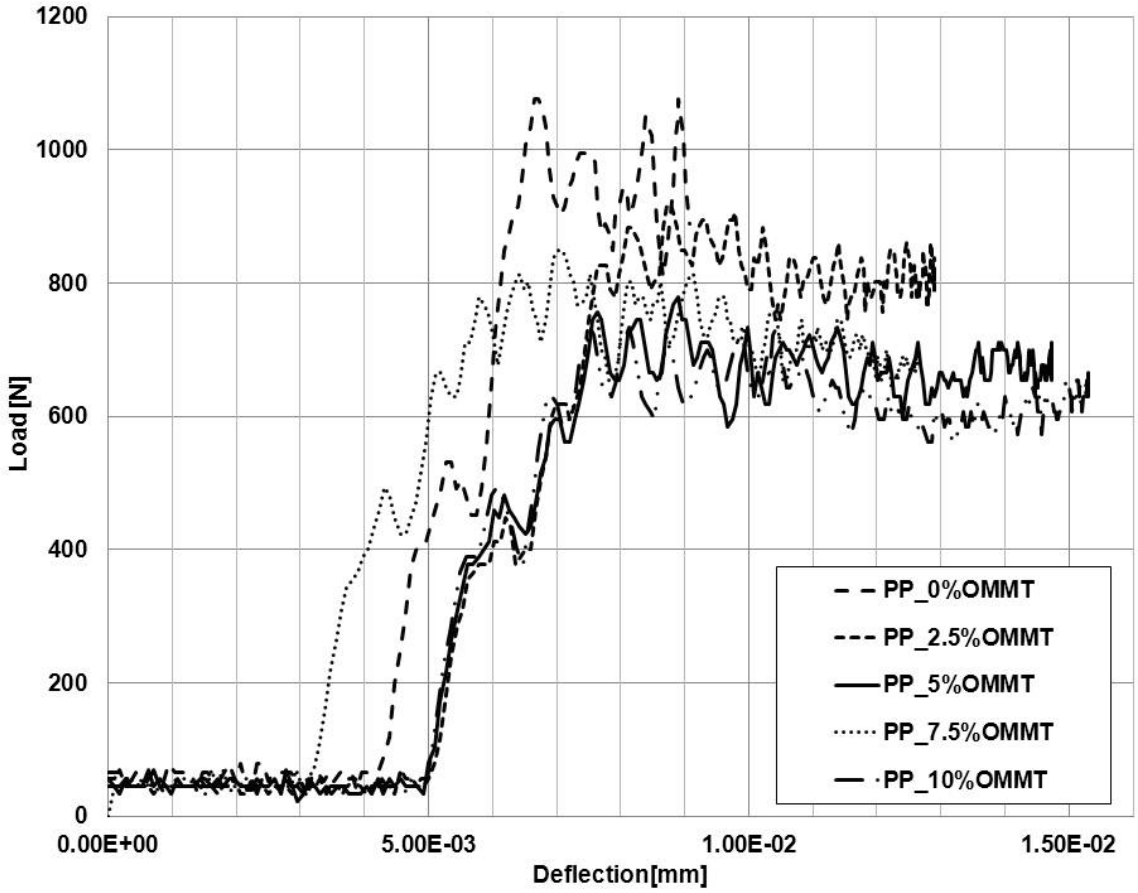

9(b) PP Point Impact

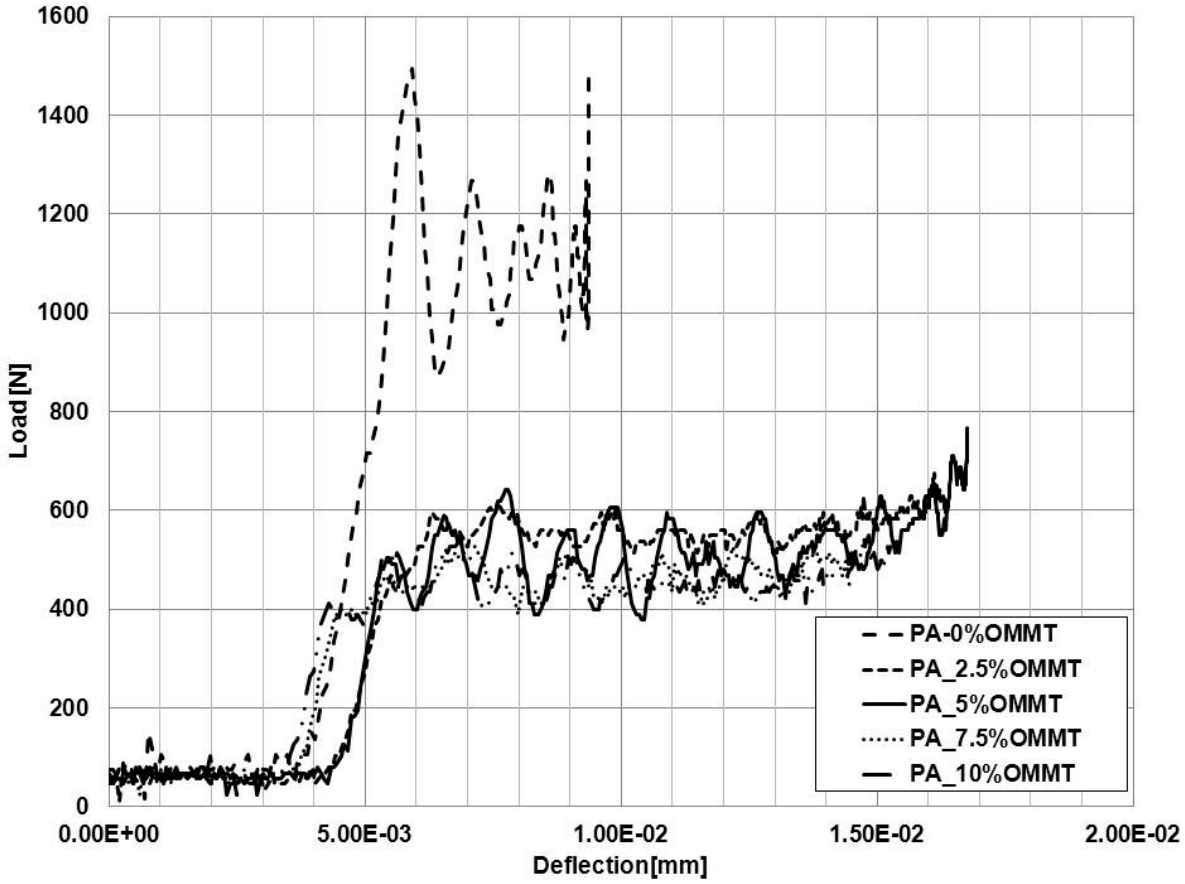

9(c) PA Surface Impact

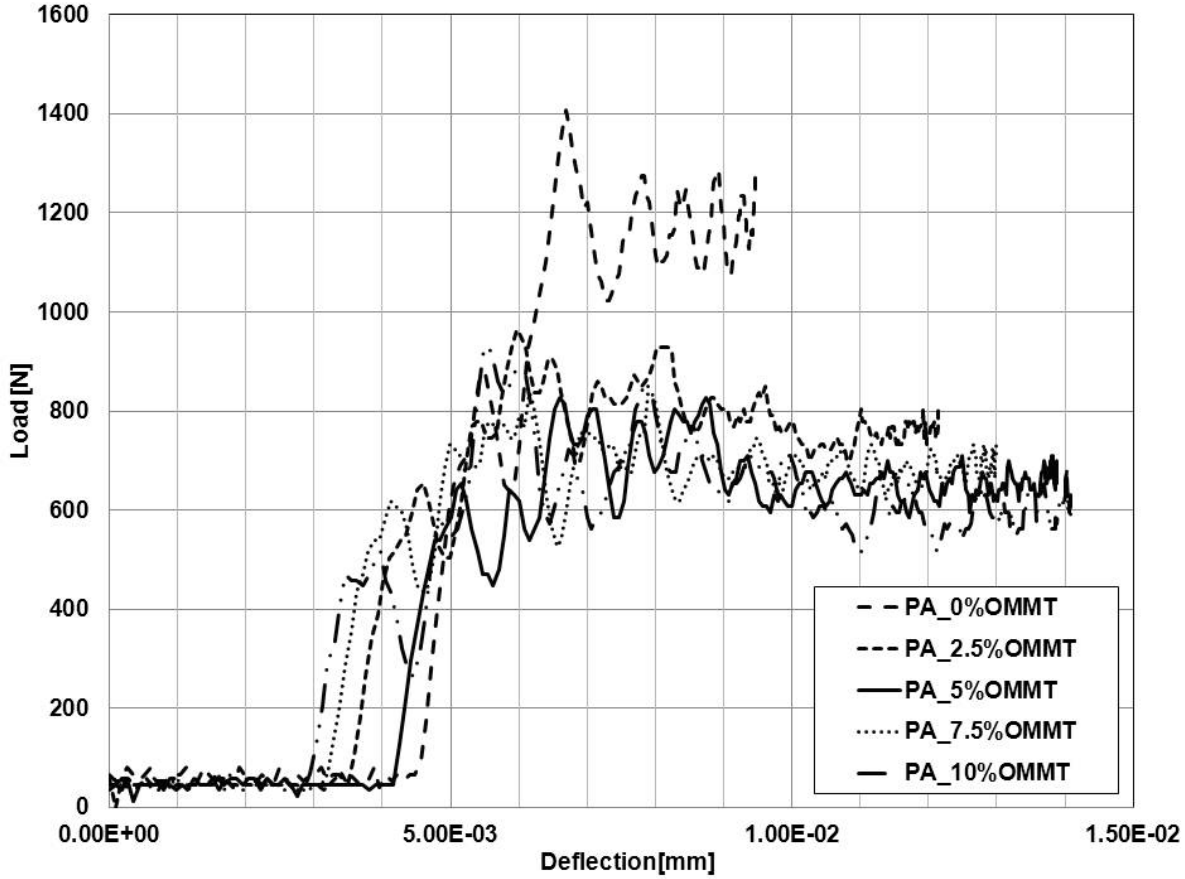

9(d) PA Point Impact

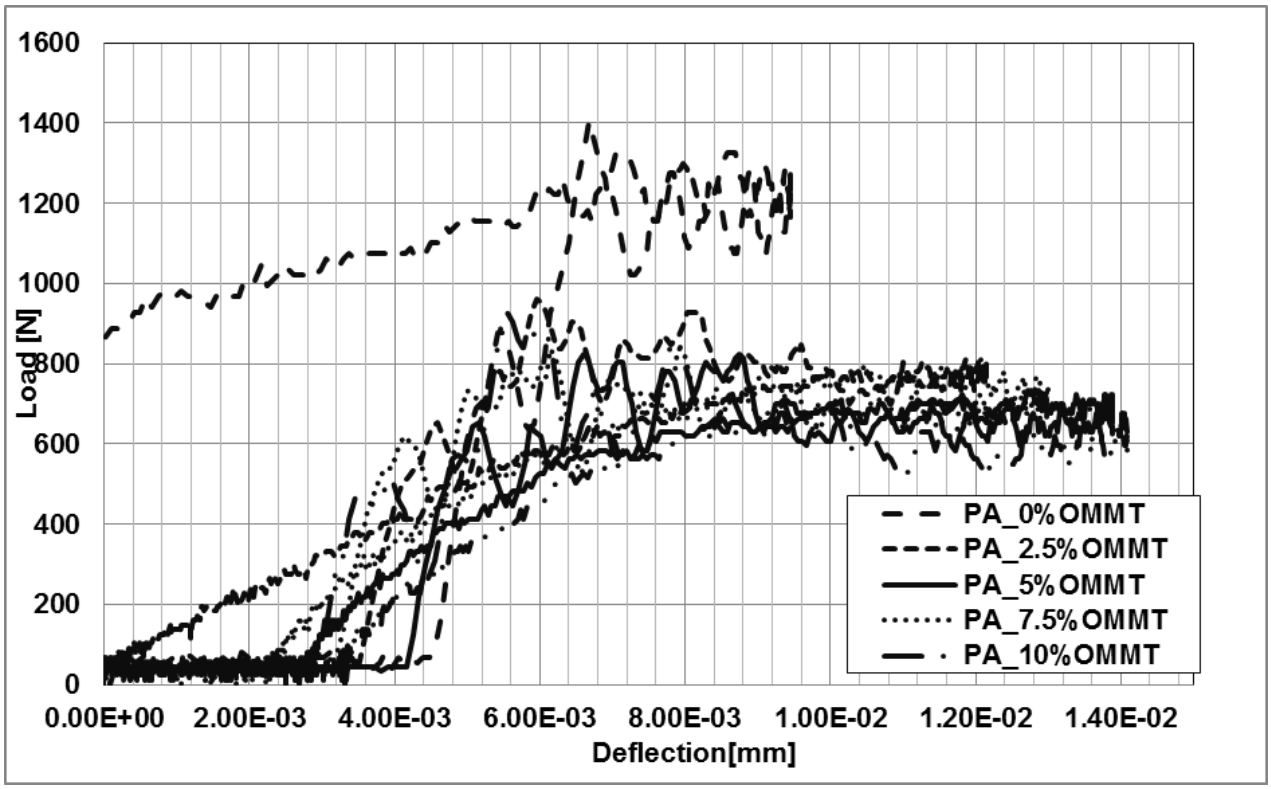

9(e) Load-deflection results for the PA point impact demonstrating the typical rebound and the force return to zero as observed for all tests conducted.

Figure 9 Load-deflection graphs for point load and surface impact. It should be noted that all the specimens reported (a-d) did not show any perforation during the impact and hence the force returned to zero for each test carried out as shown on in (e).

TABLE 1. Injection moulding parameters for face sheet manufacturing

Parameters	Material 1	Material 2
Material Code	MM PP BI24	MM PA I 1F30
Pre Drying	No	yes
Drying Temperature		90°C
Drying time		4 h
Injection mouling Machine	Ferromatik K110	Ferromatik K110
Closing Pressure	1100 kN	1100 kN
Feed Temperature	60 °C	60 °C
Temperature Zone 1	210 °C	240 °C
Temperature Zone 2	220	250 °C
Temperature Zone 3	230°C	260 °C
Temperature Zone 4	240°C	270 °C
Temperature Injector	250°C	270 °C
Tool temperature	40°C	65 °C
Melt material temperature	239°C	273 °C
Metered volume	175 cm^3	175 cm^3
Metered length	110 mm	110 mm
Rotation speed	100 1/min	100 1/min
Circumferential speed	236 mm/s	236 mm/s
Back pressure	50 mm/s	35 mm/s
Cooling time	40 s	30 s
Metered retardment	1 s	1 s
Injection pressure	1700 bar	1000 bar
Injection flow rate	100 cm^3/s	60 cm^3/s
Injection time	1.62 s	2.68 s
Switchover point	30 cm^3	30 cm^3
After-pressure	280 bar	480 bar
After-pressure time	10 s	4 s
After-pressure velocity	150 cm^3/s	50 cm^3/s
Pad	3 cm^3	1 cm^3
Comments	Screw diameter 45mm	Screw diameter 45mm

TABLE 2. Structural properties of the PU/OMMT foamed nanofoams

	OMMT content [wt. %]	Average number of cells	Average surface of cells [mm^2]*10^{-3}	Anisotropy coefficient
Parallel to direction of foam growth	2.5	84	9.4	1.45
	5	66	12	1.5
	7.5	78	10	1.41
	10	66	13	1.53
Perpendicular to direction of foam growth	2.5	89	8.3	1.21
	5	102	7.1	1.08
	7.5	98	7.6	1.07
	10	94	8.1	1.08

TABLE 3. Compression properties

Material system	Compressive Strength [MPa]	Relative de-formation εm [%]	Compressive stress (at 10%ε_m) [MPa]	Compressive Modulus [MPa]
PP PU/0%OMMT	0.236	4.76	0.229	4.55
PP PU/2.5%OMMT	0.186	4.75	0.202	3.92
PP PU/5%OMMT	0.160	3.02	0.187	5.30
PP PU/7.5%OMMT	0.183	4.56	0.185	4.01
PP PU/10%OMMT	0.139	4.56	0.162	3.05
PA PU/0%OMMT	0.270	6.53	0.263	4.14
PA PU/2.5%OMMT	0.206	4.14	00.209	4.98
PA PU/5%OMMT	0.157	3.82	0.184	4.10
PA PU/7.5%OMMT	0.163	2.99	0.189	5.45
PA PU/10%OMMT	0.149	2.63	0.172	5.67

TABLE 4. Impact performance properties

Material and impact type	Peak load (N)	Deflection at peak load (mm)	Absorbed energy (J)	Max. deflection (mm)	Impact velocity (m/s)
PP_0%OMMT_Point	1075.27	6.71	3.73	8.9	3.47
PP_2.5%OMMT_Point	917.21	8.72	5.76	12.90	3.57
PP_5%OMMT_Point	779.66	8.89	6.25	14.74	3.57
PP_7.5%OMMT_Point	848.16	6.96	6.69	12.94	3.57
PP_10%OMMT_Point	733.77	7.51	6.36	15.30	3.57
PA_0%OMMT_Point	1407.1	6.69	5.2	9.46	3.47
PA_2.5%OMMT_Point	963.07	5.96	6.54	12.15	3.57
PA_5%OMMT_Point	825.49	6.60	6.43	13.89	3.57
PA_7.5%OMMT_Point	836.95	6.15	6.61	12.99	3.57
PA_10%OMMT_Point	928.67	5.49	6.97	14.09	3.57
PP_0%OMMT_Surface	1586.69	6.73	5.04	9.48	3.11
PP_7.5%OMMT_Surface	755.24	18.10	6.38	18.10	2.64
PP_10%OMMT_Surface	869.67	17.54	5.82	17.54	2.64
PA_0%OMMT_Surface	1495.15	5.91	5.55	9.37	3.11
PA_2.5%OMMT_Surface	675.13	16.13	6.79	16.57	2.64
PA_5%OMMT_Surface	766.68	16.76	6.50	16.76	2.64
PA_7.5%OMMT_Surface	789.56	17.28	6.59	17.29	2.64
PA_10%OMMT_Surface	892.55	16.36	6.16	16.36	2.64